Aravind Baskar

Department of Aerospace and Mechanical Engineering, University of Notre Dame, Notre Dame, IN 46556 e-mail: abaskar@nd.edu

Mark Plecnik¹

Assistant Professor
Department of Aerospace and Mechanical
Engineering,
University of Notre Dame,
Notre Dame, IN 46556
e-mail: plecnikmark@nd.edu

Synthesis of Watt-Type Timed Curve Generators and Selection From Continuous Cognate Spaces

Following recent work on Stephenson-type mechanisms, the synthesis equations of Watt six-bar mechanisms that act as timed curve generators are formulated and systematically solved. Four variations of the problem arise by assigning the actuator and end effector onto different links. The approach produces exact synthesis of mechanisms up to eight precision points. Polynomial systems are formulated and their maximum number of solutions is estimated using the algorithm of random monodromy loops. Certain variations of Watt timed curve generators possess free parameters that do not affect the output motion, indicating a continuous space of cognate mechanisms. Packaging compactness, clearance, and dimensional sensitivity are characterized across the cognate space to illustrate trade-offs and aid in selection of a final mechanism. [DOI: 10.1115/1.4050197]

Keywords: mechanism design, mechanism synthesis, theoretical kinematics

1 Introduction

Timed curve synthesis refers to the design of mechanisms that trace a desired curve as coordinated with the angle of an input link. In a recent publication [1], the synthesis equations for timed curve generators for all of the Stephenson-type six-bar mechanisms were formulated, and the entirety of their solution sets were approximately computed. In this paper, the techniques introduced in Ref. [1] are extended to the Watt-type six bars, collectively covering all types of six bars with actuated base joints. Distinct from the previous work, some Watt type timed curve generators possess continuous cognate spaces, referred in literature as "Infinite Manyfoldness" [2]. This is in contrast to the more commonly addressed discrete cognates exemplified by Roberts' work on the four-bar linkage [3]. In this paper, we show how the continuous cognate spaces of Watt mechanisms can be exploited to manage trade-offs between competing design metrics. In a numerical example, we illustrate the trade-offs between link packaging, ground clearance, and dimensional sensitivity of the design as subject to manufacturing errors. The existence of continuous cognate spaces leads to additional results that expand design options. For example, a continuous space of cognates contains a point that can be classified as more than one mechanism type. This cognate can be transformed into the cognates of the new type, leading to more design options.

A schematic of a Watt-linkage is shown in Fig. 1. It consists of two ternary links and four binary links assembled in a manner that it is constituted by two independent four-bar loops. Depending on the nature of the ground link (binary or ternary), Watt mechanisms are classified as Watt I (WI) and Watt II (WII), respectively. For the Watt topology of six-bar linkages, a number of timed curve synthesis problems can be posed. Since we are studying *timed* paths, different choices of the actuator location give rise to distinct problems. In this work, we focus only on the class of problems where the actuator is located at one of the base joints for considerations of manufacturability. This narrows down the scope of the work to four distinct problems as listed in Table 1, namely, WI-A, WI-B, WI-C, and WII. The actuated link is indicated in red and the end effector point in blue. The former two cases allow a maximum of eight generic precision point specification

for which the mechanism can be designed, while the latter two cases admit only up to seven points. This distinction is due to the decoupled nature of the two independent four-bar loops in the latter cases which permits a *stretch-rotation* of one of the four-bars in them relative to the other without affecting the output motion. Thus, unlike the four-bars and the Stephenson-type six bars, certain Watt-type mechanisms offer two free design choices which manifest in the form of a choice in one of the base pivots, forming a continuous space of linkage cognates.

2 Literature Review

Recent research in exact kinematic synthesis has been driven by the development of powerful tools in numerical algebraic geometry [4–6]. This is because the commonly used kinematic lower pairs are conveniently represented by algebraic constraints, forming polynomial systems. Apart from numerical continuation, several techniques demonstrated the design of linkages, often four-bars, using closed form expressions [7,8] to identify all solutions to a set of synthesis equations. In the absence of closed form expressions, researchers have employed various optimization techniques to design four- and six-bar linkages [9–11]. The advantage of obtaining all synthesis solutions from the designer's perspective is to generate a large pool of options for a given specification. Numerical continuation has enabled this strategy to be applied to larger, highly nonlinear systems where closed form expressions are practically impossible [12–14].

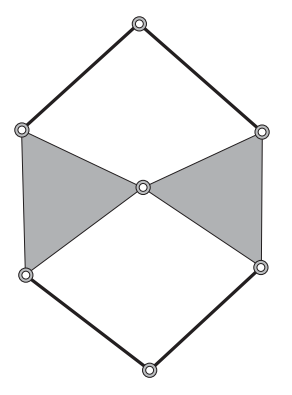


Fig. 1 Six-bar linkage of Watt-type

¹Corresponding author.

Contributed by the Mechanisms and Robotics Committee of ASME for publication in the JOURNAL OF MECHANISMS AND ROBOTICS. Manuscript received August 13, 2020; final manuscript received January 26, 2021; published online May 20, 2021. Assoc. Editor: Xianwen Kong.

Table 1 Timed curve synthesis of Watt-type six-bar mechanisms

Name	Watt I (WI-A)	Watt I (WI-B)	Watt I (WI-C)	Watt II (WII)		
Description						
Precision points Number of free parameters Root count estimate ^a	8 - 237,566×4	8 - 1,104,140×2	7 2 $101,054 \times 1$	7 2 $12,360 \times 2$		

⁻ Actuated link; • End-effector point.

Root count represents a high ceiling for the maximum number of solutions possible in each case.

Root count estimate = $g \times c$, where g = #groups, c = #cognates.

In much of these works, emphasis has been on designing mechanisms for functions, paths, and motions. Timed curve synthesis involves coordinating a path with an input angle. This coordination can deliver required force transmission characteristics while the desired path is being traced. In the domain of four-bars, a few references that address timed motion can be found in the literature [9,15]. The need for specifying greater number of precision points requires the exploration of six-bar design space. Approximately complete solution sets to timed curve synthesis equations of Stephenson-type six bars has recently been solved [1,16]. This work extends those results to Watt-type six bars.

The availability of two free choices in certain Watt mechanisms makes it possible to study the solution space for optimal design characteristics which are secondary to the input specification. In this work, we consider a few secondary considerations, including the sensitivity of the output task to dimensional errors. Lee et al. [17] and Hanzaki et al. [18] have also produced synthesis method that explicitly consider dimensional sensitivity. We employ a two-staged design process. First, we synthesize WI-C mechanisms for a given input specification using parameter homotopy and then study the free space of two dimensions to arrive at optimal designs for packaging requirements and dimensional sensitivity.

3 Mathematical Formulation

The timed curve synthesis problems in the Watt linkages are formulated in this section. The schematics are shown in Table 2. WI-A and WI-B differ only by the choice of input and are combined in Table 2 for concise representation. The goal is to formulate a system of equations from first principles. The steps adopted here follow the recent work on Stephenson linkages [1] with some notable changes.

In each case, the reference configuration of the mechanism is chosen such that the end effector corresponds to the initial precision point P_0 . The pivots and the end effector tips are labeled as shown, namely, A, B, C, D, F, G, H, and P, respectively. We then consider a displaced configuration where the end effector visits the precision point P_j . The displaced angle of each of the moving links between the two configurations are labeled using ϕ_j , ρ_j , ψ_j , θ_j , μ_j , and ν_j as shown in the schematics. Note that there are only five displaced angles in each case, and we adopt a slightly modified convention for each.

The mechanism is drawn in the *complex* plane where each pivot location is represented as a complex position vector. This notation called the *isotropic coordinates* [19] offers multiple advantages in view of the numerical technique we use. The angular displacements must also be represented as complex numbers for consistent representation. We introduce the following *rotation operators* to achieve this

$$Q_j = e^{i\phi_j}, \quad R_j = e^{i\rho_j}, \quad S_j = e^{i\psi_j}$$

 $T_i = e^{i\theta_j}, \quad U_i = e^{i\mu_j}, \quad V_i = e^{i\nu_j}$

where $i = \sqrt{-1}$ is the imaginary unit.

With the notation defined as above, vector loop equations can be written in each case between the two configurations. All the vector loops initiate from one of the ground pivots, running through the two precision points P_0 and P_j and terminating back at the same ground pivot. Three independent vector loops are written in each case which is the maximum number of independent loops possible. All the pivot locations and the rotation operators with the exception of the one corresponding to the input link are variables in the formulation, while the precision points and the input rotation operator are specified design parameters.

Conjugates of the vector loop equations must also be considered because a complex variable and its conjugate are treated independently in the isotropic coordinates representation. Thus, the conjugate of a pivot location is considered a distinct variable. For the rotation operator variables though, the conjugates are their respective reciprocals by definition. These reciprocals result in equations containing fractions which are cleared using appropriate multipliers to obtain the equations in polynomial form. To demonstrate, the conjugate equation of the third loop of the WI-C mechanism is

$$B^*S_iV_i + (G^* - B^*)V_i + (P_0^* - G^*)S_i = P_i^*S_iV_i$$
 (1)

The maximum number of generic precision points for which the Watt linkages can be synthesized has to be determined. Unlike the Stephenson linkage where a maximum of eight points can be specified in all its cases [1], the WI-C and WII mechanisms can be designed for a maximum of seven precision points but allow two free parameters. This can be shown by checking for equation independence in the square systems formed by WI-C and WII and is geometrically understood by the existence of a stretch rotation of one of the component four-bars that renders the output motion unchanged. Simple arithmetic analysis shows that for WI-A and WI-B, the formulation results in a full-rank square system² of dimension 42 for eight precision points $(P_0, P_1, ..., P_7)$. This analysis is explained in detail in the context of Stephenson linkages [1] and is omitted here. This completes the formulation of the system of equations for WI-A and WI-B.

In order to solve synthesis equations for WI-C and WII, two free dimensions must be specified. This can be done many different ways and has ramifications on the amount of floating point precision required for the proceeding numerical homotopy tracking. Dijksman [2] has suggested the specification of ground pivot A in

^aFor the cases WI-C and WII, the root count estimates presented correspond to a generic choice of the two free parameters.

²A square system of equations is a system with an equal number of equations and variables.

Table 2 Mathematical model of Watt-type six-bar mechanisms for timed curve synthesis

Schematic Mathematical model^a WI-A & WI-B Input WI-A Input WI-B $A + (C - A)R_i + (F - C)T_i + (P_0 - F)U_i = P_i$ $B + (D - B)S_i + (F - D)T_i + (P_0 - F)U_i = P_i$ $B + (G - B)S_i + (H - G)V_i + (P_0 - H)U_i = P_i$ Parameters: $\{P_0, P_i, \mathbf{M}_i\}$ Variables: $\{A, B, C, D, F, G, H, \mathbf{N}_i, T_i, U_i, V_i\},\$ where the definitions of M_i and N_i are as follows. Case $\overline{\text{WI}} - \text{A}$ R_i WI - B S_i WI-C $A + (C - A)R_j + (F - C)T_j + (H - F)U_j + (P_0 - H)V_j = P_j,$ Input $A + (C - A)R_j + (D - C)T_j + (G - D)S_j + (P_0 - G)V_j = P_j,$ $B + (G - B)S_i + (P_0 - G)V_i = P_i$. Extra constraint: $(D - B) = \tau(G - B)$. Parameters: $\{P_0, P_i, R_i, \tau\}$ Variables: $\{A, B, C, D, F, G, H, S_j, T_j, U_j, V_j\}$ WII $B + (A - B)Q_i + (C - A)R_i + (F - C)T_i + (P_0 - F)U_i = P_i$ Input $D + (F - D)T_i + (P_0 - F)U_i = P_i$ $G + (H - G)V_i + (P_0 - H)U_i = P_i$ Extra constraint: $(C - D) = \tau(F - D)$, Parameters: $\{P_0, P_j, Q_j, \tau\}$ Variables: $\{A, B, C, D, F, G, H, R_j, T_j, U_j, V_j\}$

WI-C to resolve the ambiguity. In this work, we make the system square by adding an extra constraint as shown in Table 2. In WI-C, the extra constraint specifies the shape factor (τ) of the triangular link BDG. It represents the relative stretch-rotation of vector DB with respect to GB. Similarly, in WII, a constraint that fixes the vector CD in relation to FD is specified. Naturally, the conjugate

equation of these constraints must also be included. This yields a square system of dimension 38. The stretch factor that denotes the magnitude of τ and its conjugate τ^* is chosen close to unity. We discuss the numerical advantage of this strategy in Sec. 5. With this final step, the formulation of WI-C and WII problems is also completed.

^aThe usage of isotropic coordinates involves additional conjugate equations and variables which are not printed for brevity. They follow the form shown in Eq. (1).

Table 3 Cognates of Watt-type timed curve generators

	Cognate constructions	Solution group
WI-A & WI-B	$\Lambda(\mathbf{X}) := \{ \xi(A), B, \xi(C), B + F - D, F, \zeta(G), \zeta(H), P_0 \},$ where $\xi(z) = \frac{F - D}{C - D}(z - B) + B$, and $\zeta(z) = \frac{B - D}{G - D}(z - F) + F$.	$ \frac{\text{Case WI-A}}{\begin{cases} \mathbf{X} \\ \Lambda(\mathbf{X}) \\ \Gamma(\mathbf{X}) \\ (\Lambda \circ \Gamma)(\mathbf{X}) \end{cases}} $
	$\Gamma(\mathbf{X}) := \{ \chi(A), B, \chi(C), \kappa(D), \kappa(F), G, G + P_0 - H, P_0 \},$ where $\kappa(z) = \frac{P_0 - H}{F - H}(z - G) + G$, and $\chi(z) = \frac{\kappa(D) - B}{D - B}(z - B) + B$.	$\frac{\text{Case WI-B}}{\left\{ \begin{array}{c} \mathbf{X} \\ \Gamma(\mathbf{X}) \end{array} \right\}}$
WI-C	$\Omega(\mathbf{X}, \sigma) := \{ \xi(A), B, \xi(C), \xi(D), \zeta(F), G, \zeta(H), P_0 \},$ where $\xi(z) = \sigma(z - B) + B, \zeta(z) = \frac{\sigma(D - B) + B - G}{D - G}(z - G) + G,$	$\{\Omega(\mathbf{X},\sigma)\}$
WII	and σ is the complex stretch-rotation parameter of two free choices. $\Omega(\mathbf{X}, \sigma) := \{\xi(A), \xi(B), \xi(C), D, F, G, H, P_0\},$ where $\xi(z) = \sigma(z - D) + D$, and σ is the complex stretch-rotation parameter of two free choices. $\Lambda(\mathbf{X}) := \{\chi(A), \chi(B), \chi(C), \kappa(D), \kappa(F), G, G + P_0 - H, P_0\},$ where $\kappa(z) = \frac{P_0 - H}{F - H}(z - G) + G$, and $\chi(z) = \frac{\kappa(F) - \kappa(D)}{F - D}(z - D) + \kappa(D).$	$\left\{ \begin{aligned} &\Omega(\mathbf{X},\sigma) \\ &\Lambda(\Omega(\mathbf{X},\sigma)) \end{aligned} \right\}$

Note: For any mechanism design given by the architecture variables in lexicographical ordering $X := \{A, B, C, D, F, G, H, P_0\}$, the cognate constructions are presented here following the same order of the architecture variables of the respective linkage (refer the figures in Table 2.).

4 Solving Polynomial Systems Using Monodromy Loops

The system of equations derived in the earlier section are polynomial in nature. An advantage of polynomial formulations is that the equations possess a finite number of roots, referred to as the *root count* of the system. The first step (or the ab initio step) in solving these systems is finding the root count through a numerical continuation run. Several techniques in numerical algebraic geometry have been developed to enable this step. Techniques such as multi-homogeneous homotopy and regeneration homotopy were used in the last decade to solve function generation problems for six-bar linkages [14,20]. Because of the occurrence of a large number of divergent paths, iterative techniques that generate roots starting from a small subset assumed prominence in the recent years [1,21–24]. The application of random monodromy loops (RML technique) is one such technique and is described later.

4.1 Random Monodromy Loops. Let the polynomial system of equations be defined by $\mathbf{F}(\mathbf{z}, \mathbf{p}) = \mathbf{0}$, where \mathbf{z} is the set of variables and \mathbf{p} is the set of parameters/constants. The algorithm requires at least one start solution to initiate the iterations. Each iteration of the algorithm involves the creation of an auxiliary system $\mathbf{F}(\mathbf{z}, \mathbf{p}_{\gamma}) = \mathbf{0}$ with a randomly chosen set of parameters \mathbf{p}_{γ} . The original system is deformed into the auxiliary system, then back into the original system according to the equation,

$$\mathbf{H}(\mathbf{z}, t) := \mathbf{F}(\mathbf{z}, \mathbf{p})(1 + e^{it}) + \mathbf{F}(\mathbf{z}, \mathbf{p}_{y})(1 - e^{it}) = \mathbf{0}$$
 (2)

by incrementing t from 0 to 2π . During this deformation, the accumulated roots are tracked using the Bertini homotopy tracking module [25]. Each orbit out to a random system returns paths to a permuted set of roots, a subset of which will be newly accumulated roots. The first few iterations of RML accumulate roots quickly and last few converge on the root count of the system. The model of the progression follows Lincoln-Petersen model which is based on the percentage of repeated solutions in an iteration as described in

Ref. [26]. In the same study, it has been demonstrated using a statistical analysis that monodromy technique leads to robust estimates of the root count.

4.2 Cognates of Watt Linkages. Solutions to some kinematic synthesis equations occur in groups called *cognates*. Cognate groups indicate linkages of dissimilar dimensions that possess some identical relevant slice of their configuration space. The prototypical examples of linkage cognates are Roberts' cognates of the four-bar. Hence, if one solution satisfies the system of equations, the others in the group must exist as well. One of the key features of the RML technique and the root generation techniques in general is that if the polynomial system admits group solutions, it can be exploited to reduce the computational effort required for the ab initio step. The existence of Watt cognates was listed in Dijksman's work [2], which has also been validated recently [27]. In Table 3, we have provided algebraic rules to compute the cognates given a candidate.

Cognates in Watt linkages can be classified into two kinds. The first is the *discrete* cognates that occur as isolated members (denoted by Γ and Λ in Table 3). WI-A, WI-B, and WII admit such kind of cognates. WI-C and WII admit a second kind denoted by Ω that occur as a *continuous* family of cognates with σ as the complex stretch-rotation parameter. These continuous cognates share an identical slice of the input–output configuration space just like a set of discrete cognates. The occurrence of this family of cognates can be attributed to the existence of two four-bar loops in Watt linkages. In WI-C and WII, the location of actuators and end effectors is such that the actuated four-bar acts as a function generator in a serial manner over the other four-bar that contains the end effector. It is well-known that function generators are unaffected by stretch and rotation—hence, the complex stretch-rotation parameter σ .

For the ab initio computation, the size of the set of discrete cognates reduces the convergence limit by that factor, resulting in computational savings. WI-A is reduced by a factor of 4, and WI-B and WII are reduced by a factor of 2. Members of a cognate

Table 4 Design specification for the numerical study

	P_0	P_1	P_2	P_3	P_4	P_5	P_6	P_7
X + Yi (m)	0	-0.0038 +0.0105i	-0.0074 +0.0177i	-0.0175 +0.0250i	-0.0270 +0.0187i	-0.0345 + 0.0078i	-0.0434 -0.0088i	-0.0599 -0.0372i
α (rad)	0	0.2398	0.5857	1.3963	1.8621	2.2689	2.7110	3.3161

Note: The parameters are as follows: X and Y coordinates of the path points and the corresponding angular displacement α of the input link from the reference configuration. For WI-C and WII cases, the precision point P_5 is omitted from the design specification.

Table 5 Summary of the parameter homotopy computations and the post-processing steps

				No. of linkages free of all kinematic defects			
	No. of paths tracked	Percentage of successful paths (%)	No. of physical linkages	8 position	7 position	6 position	5 position
WI-A	237,566	56.57 ± 0.27	3463 ± 834	2 ± 3	3 ± 3	40 ± 14	156 ± 60
WI-B	1,104,140	38.03 ± 0.10	6487 ± 572	2 ± 2	12 ± 7	75 ± 29	279 ± 86
WI-C	101,054	74.01 ± 0.22	1197 ± 156	_	0 ± 0	4 ± 2	37 ± 18
WII	12,360	76.95 ± 0.05	334 ± 43	-	0 ± 0	0 ± 0	5 ± 3

group of the discrete kind are considered as one entity during the ab initio run. A similar reduction was available for Stephenson linkages in Ref. [1].

4.3 Computational Details. A generic system is formed for each problem. The parameter values can be randomly specified as complex numbers. We do not impose the conjugate relations of the parameters for the ab initio runs. Note that the conjugate relationship on the design parameters is not adhered to only for the ab initio problem.³ With an initial start solution, homotopy continuation iterations are carried out using the software Bertini [6,25] in parallel mode on a Intel Xeon 2.30 GHz system with 192 cores in the Center for Research Computing at the University of Notre Dame. We use double precision of 64 bit for most of the iterations and 128 bit for the final few in each case. This strategy bias our implementation toward speed for the bulk of iterations, then toward accuracy for the final few iterations. About 5% of paths resulted in numerical failure with 64 bit precision versus <1% for 128 bit precision. The failed solutions of initial iterations are highly likely to be picked up in subsequent iterations. The convergence limit of RML provides an accurate estimate of the ultimate root count of the system. These final converged estimates are reported in Table 1. WI-B admits the highest number of solutions (more than a million) to a generic specification. Note that this indicates the number of complex solutions and not of physical linkages, which tend to be a small subset. The WII system computed the fastest in 10 min. WI-B computed the slowest over 2 days to reach its convergence limit. This striking difference in the computation time is attributed to disparity in the root count of the corresponding systems. The solution sets computed are sufficient to find candidate designs for practical applications via parameter homotopy which is demonstrated in Sec. 5.

5 Numerical Examples

For the numerical study, we present a design problem defined by the precision points shown in Table 4. The home precision point P_0 is assumed to be the origin without loss of generality and the other

design points are referenced with respect to the origin. Similarly, the angular displacement of the input link is also measured relative to the home configuration, which is unknown yet. In each case, the direction of input motion could be clockwise or counter-clockwise leading to two variations. It may be noted that the phase of motion between the precision points P_0 and P_3 is about 80 deg. We consider two other variations instead (not shown in Table 4) where this phase of motion is 40 and 20 deg, respectively, totaling six sub-problems in each of the four cases WI-A, WI-B, WI-C, and WII, respectively. For WI-C and WII, the precision point P_5 is omitted because of the natural restriction that limits the number of generic precision points to seven. We are interested in identifying fully mobile mechanisms containing at least five precision points in a configuration *circuit* [28] and delivering desirable motion through a cycle of 2π radians.

In order for numerical computations to proceed for the WI-C and WII cases, first a member of its two parameter continuous cognate space must be selected. We investigated two such selection strategies. First, we considered specifying a ground pivot (A for WI-C and B for WII). This lead to a high failure rate of about 50% during homotopy path tracking. An alternative strategy was then formed by specifying the shape factor τ of the triangular link (τ =i and τ =1 for WI-C⁴ and WII, respectively, refer Table 2), reducing the failure rate to 5%. We theorize that the second strategy does a better job keeping numbers near unity in order to reduce the floating point precision requirement.

The design specifications decided above represent parametric variations of the generic systems solved in the ab initio runs and form the *target* system. Then, the *parameter homotopy* technique provides a means for deforming generic systems into target examples [6]. We execute parameter homotopy runs using Bertini in 64-bit precision to find numerical solutions to the target system. A consistent percentage of solution paths failed due to numerical issues typical to homotopy path tracking. We report the success percentage of the homotopy paths in Table 5. As six subproblems are solved in each case, we represent the entries as $AM \pm SD$, where AM is the arithmetic mean and SD is the standard deviation of the respective entries.

The source(s) of the failure rates displayed in Table 5 are not entirely clear. However, they can seemingly be explained by our choice of parameter space for the ab initio problem. Ab initio start

³This structure is avoided for the time being in order to keep our computed solution set numerically general. During subsequent computations, parameter sets specified with conjugate relationships are less general and therefore encompassed by our ab initio computational work.

 $^{^4}For$ WI-C case, the natural choice $\tau\!=\!1$ fails because of a degeneracy whereby the floating loop DGHF collapses to a point.

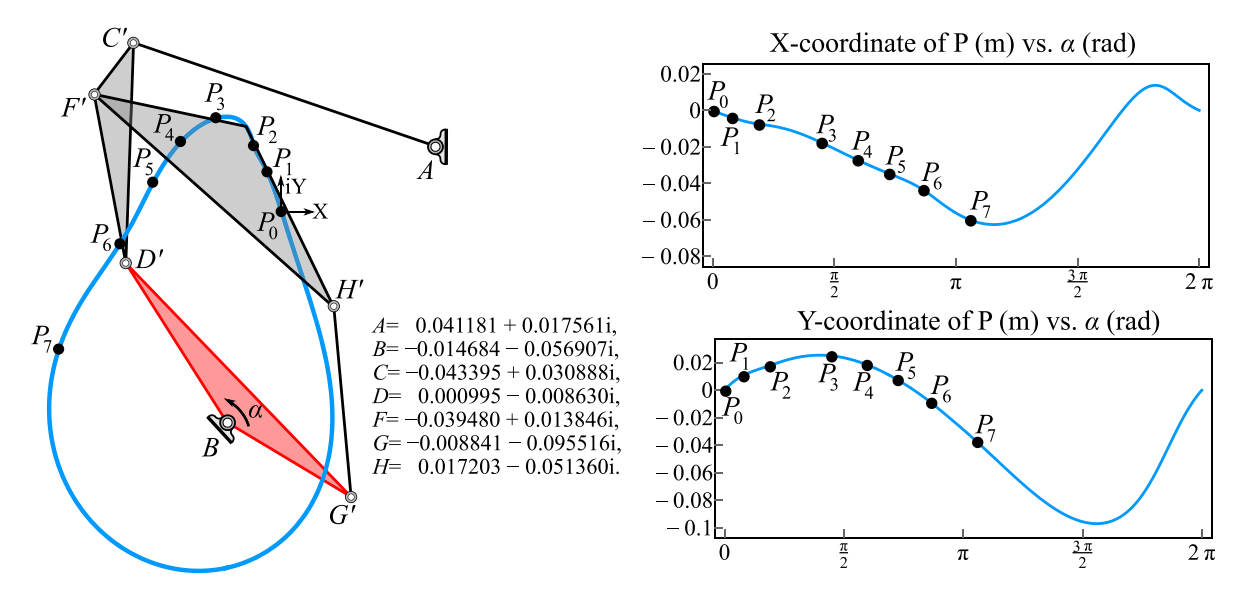


Fig. 2 A design candidate from the WI-B pool of solutions showcasing the desired output motion. Only the relevant output circuit is shown here. The pivot location numbers presented correspond to the home configuration P_0 and not the depicted one.

parameters were chosen such that rotation operator pairs, e.g., (Q_j, Q_j^*) , were independent. For short, we will call these sets Type A. For physical problems, these parameter sets deform during homotopy into final sets where Q_j and Q_j^* are reciprocals. For short, we will call these Type B. Since Type A parameters are more generic than Type B parameters, they can be expected to correspond to systems with more or the same number of solutions than systems constructed from Type B parameters. Therefore, enforcing Type B parameters during an ab initio computation might result in a tighter solution count. Despite this potential benefit, Type B parameters greatly raise numerical precision requirements and computational time. Therefore, Type A ab initio sets were chosen because they present more tractable calculations, for the trade-off of having slightly inflated solution counts.

An examination of the WII solution sets provides evidence to the theory above. The WII case was inspected because its small size made investigative computations tractable. A WII system was constructed from Type B parameters, and 9,578 solutions were found using 1024-bit precision. The computation was 50 times slower than the original (Type A) ab initio computation, which found 12,360 solutions. The reduction in solution counts, 9,578/12,360=77.49%, can be compared to the WII success rate of 76.95% displayed in Table 5.

Further evidence that a Type B parameter set would reduce the solution count from Type A comes from accounting monomials. It can be shown that if an additional elimination step were performed on the equations of Table 2, and the reciprocal relation $Q_j^* = 1/Q_j$ was enforced, then the monomial $AA^*T_jU_j$ would vanish. The additional step eliminates R_j from the first WII equation in Table 2.

In summary, a Type B parameter set most likely would reduce solution counts, but at the expense of making computational work intractable. Despite yielding reduced solution counts for generic ab initio systems, for the parameter homotopies leading to physical systems, both Type A and Type B start systems should lead approximately to the same solution sets. This theory also applies to the synthesis of Stephenson timed curve generators [1].

5.1 Post-Processing Steps. In the first step, solutions that correspond to physical linkages are identified. This is done by comparing the values of each variable and its "conjugate" counterpart to

ascertain if they form an actual complex-conjugate pair. The same can also be done by checking if the magnitude of all rotation operator variables are unity within an error limit.

The direct kinematics of Watt linkages can be solved one loop at a time, admitting a maximum of four solutions. For instance, in WI-A case, given the input angle, the assembly configurations (elbow-up and elbow-down) of the four-bar ACDB can be first solved, and the dyad FHG can be solved subsequently (elbow-up and elbow-down). Existence of these modes gives rise to the possibility of branch defects and circuit defects [28]. Solutions that do not contain at least five precision points in the same elbow modes are rejected. We allow for some precision points to skip the desired mode because design practice shows that solutions with even only five of the eight desired points are potentially useful. Note that the solutions that pass this filter could still be defective and are subject to further investigation as follows.

For the six-bar Watt mechanism to be fully mobile, it is a necessary but not a sufficient condition that the actuated four-bar (ACDB in WI and BACD in WII-refer Table 2) is fully mobile. In other words, we are looking to identify the solutions with crank-rocker or double-crank type actuated four-bars. Conditions based on the link dimensions to identify such four-bar types are welldocumented in the literature, see Ref. [29]. The final step is then to verify that there are no locking configurations (where FH and HG align) in the other loop (FHG) for mobility considerations. This can be analytically done based on the link dimensions by computing the locking configurations of the mechanisms explicitly and verifying them against the desired elbow mode of the actuated four-bar to ensure they do not match. In other words, it is necessary that the locking configurations even if they exist do not occur in the desired circuit. Solutions that pass all these checks contain precision points in the specified order inherently as they are timed. In Table 5, the breakdown of these steps is described in terms of the number of physical linkages including the discrete cognates and the subset of linkages that are defect-free while containing 8, 7, 6, and 5 precision points, respectively.

The direct kinematics of a Watt six-bar breaks into two sequential four-bar mechanisms, providing closed-form expressions which enable fast defect analysis routines [28,30]. This is an advantage over Stephenson mechanisms which necessitate a more computationally demanding routine [1,13,14] due to their inclusion of a five-bar loop.

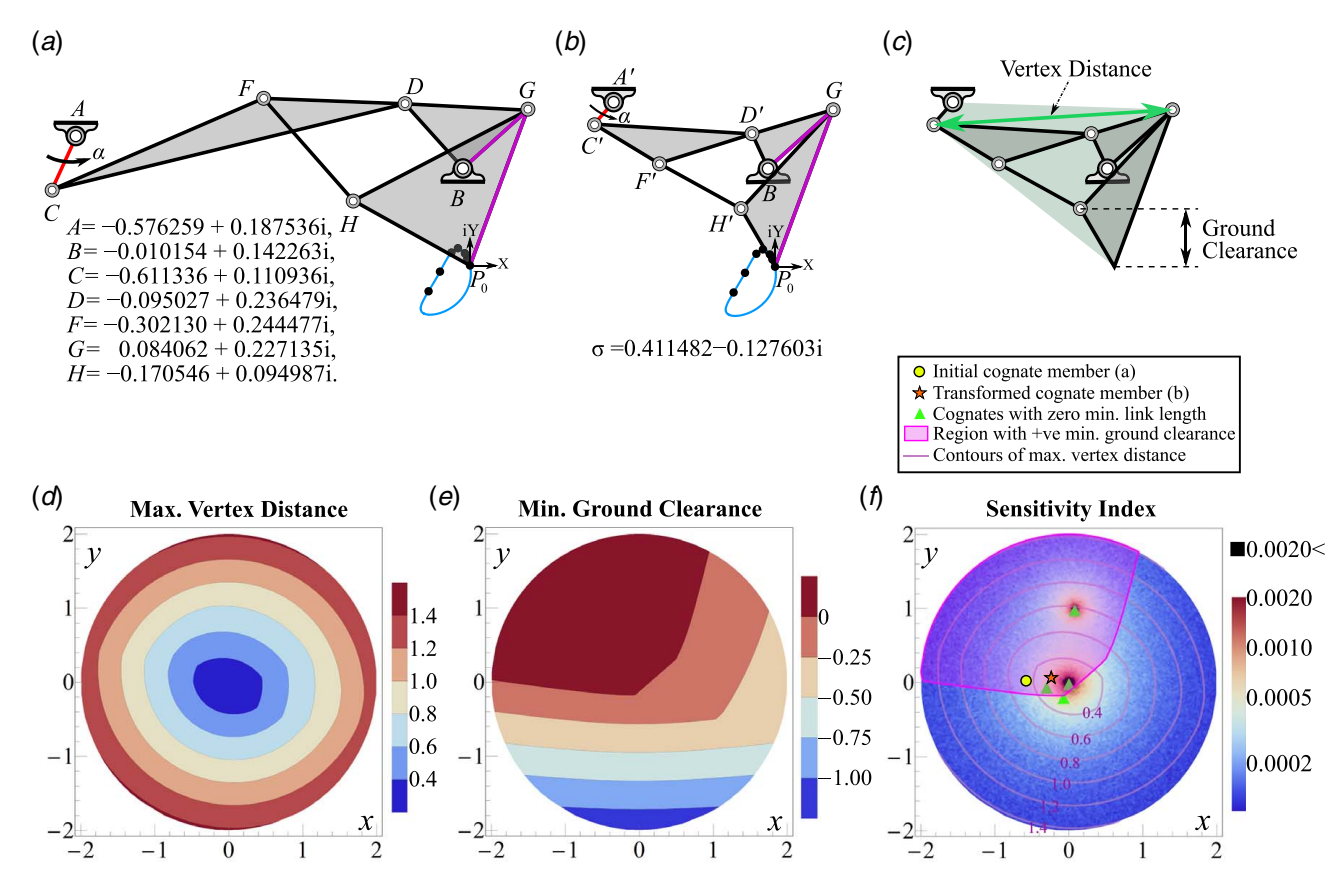


Fig. 3 (a) Watt I-C feasible design computed for the specification in Table 4. (b) A cognate in the parametric family of the design following the rule in Table 3. (c) A pictorial representation of the design traits studied, namely, vertex distance and ground clearance. (d) Contour plot of the maximum vertex distance among the continuous family of cognates. (e) Contour plot of the minimum ground clearance among the cognate family. (f) Density plot of sensitivity index with the contour lines of max. vertex distance and min. ground clearance superimposed.

6 Eight Position Synthesis

Figure 2 is a WI-B design that produces desirable motion. All the eight precision points are present in the circuit of interest as indicated in the configuration space plots x versus α and y versus α . We note that for the application considered, it is preferable to have all the pivots (moving and fixed) located above the end effector point throughout the cycle of motion for ground clearance. It follows that the location of fixed pivot B is undesirable. For the WI-A and WI-B cases, the link dimensions cannot be tuned without affecting the input—output motion. While it is possible to relax a precision point requirement in order to address secondary considerations such as the need for ground clearance, this would require a sizable amount of extra computation to perform, on the

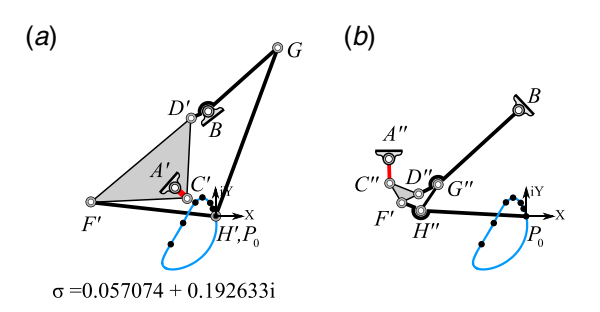


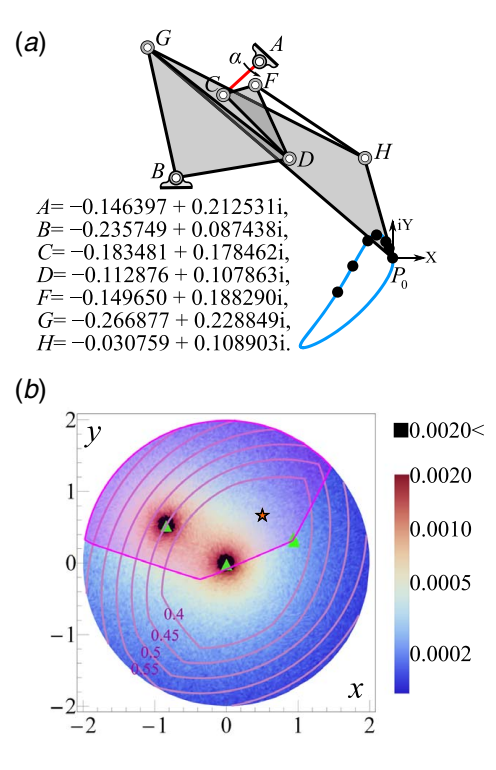
Fig. 4 Illustration of the confluence between WI-A and WI-C mechanisms. Part (a) shows a WI-C cognate of the design in Fig. 3(a). It is also a WI-A type mechanism as P_0 is common to both the links GH' and F'H'. Because of this, WI-A cognate shown in part (b) is also a potential design solution.

order of hours or days. The extra computational work would involve varying parameter sets, computing a parameter homotopy for each variation, and then processing the results. In comparison, the continuous cognate families of WI-C and WII are defined by simple closed-form equations that can be used to immediately explore the variation of two free design parameters. We demonstrate this using WI-C examples in the following. The general principles hold true for WII case as well.

7 Seven Position Synthesis With Free Parameters

Consider an example design of WI-C mechanism shown in Fig. 3(a). Its coupler path is mostly desirable, missing P_2 and P_4 by an imperceptible margin, but its links are disproportionately large. However, Fig. 3(a) displays just one member of a broader continuous family of WI-C cognates. Another member is displayed in Fig. 3(b), which is more compact. In order to knowledgeably select a design from this two dimensional space of cognates, we considered three secondary metrics: link compactness, ground clearance, and dimensional sensitivity. For this study, we identify the cognates by the relative positioning of ground pivot A from B in terms of x and y coordinates. All allowable changes follow the constructions shown in Table 3. Note that the location of B, G, and P_0 (indicated by connected purple lines in Figs. 3(a) and 3(b)) are invariant of the cognate transformation Ω . In other words, the location of B and G in all configurations must be acceptable to begin with.

1. Max. Vertex Distance: As a measure of compactness of a design, we first compute the largest distance between any two of the vertices A, B, C, D, F, G, H, and P in a given configuration. For instance, in the configuration of the design in Fig. 3(b), the



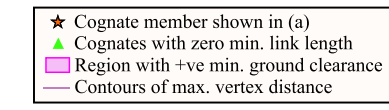


Fig. 5 Another feasible design solution to the target specification. Part (a) shows the design selected from the grid analysis and part (b) shows the combined contour plots of the design traits

distance C'G is the largest which is indicated in Fig. 3(c). Then, the maximum of the vertex distance across all the configurations through the input motion of 2π radians is found. This computation is carried out at a resolution defined by 40 discrete set of input values at equal step size in WOLFRAM MATHEMATICA [31]. In Fig. 3(d), the result of this analysis is shown via a contour plot. Coordinates of the plot indicate the relative position of the ground pivot A with respect to B, which is a constant for all cognate designs in this family. We use a rectangular grid consisting of 20,172 nodes within a radius of 2 m at a resolution of 0.025 m. For a compact design, the smaller the max. vertex distance the better the design. While it is obvious that the max vertex distance increases as A moves away from the location of B, the analysis of this family shows a bias in which it is favorable to position A horizontally outwards, see Fig. 3(d).

2. Min. Ground Clearance: The path generated for this example has utility as a leg mechanism for a hopping robot. Therefore, as a second metric we consider the distance at which its joints would clear the ground over its motion cycle. Ground clearance is defined as the minimum vertical displacement of all pivots A, B, C, D, F, G, H from the end effector point P. Refer Fig. 3(c) for a graphic illustration. We record the minimum of this value across 40 configurations of the input motion as earlier. A design is fit if the min. ground clearance value is positive. The upper contour of Fig. 3(e) represents acceptable regions of the continuous cognate space.

3. Sensitivity Index: Finally, sensitivity of the design output to errors in manufacturing is studied. For each member in the grid, we perturb the location of the pivots in their respective

neighborhoods of the home configuration via a multi-normal distribution of sample size 50 with a constant diagonal co-variance matrix of value 1.6×10^{-8} . This is chosen to correspond to standard CNC machining tolerance. The total average error in the output path of the perturbed designs from the ideal one is recorded through 40 discrete timed points of the input cycle in each case and is defined as the *sensitivity index*. Figure 3(f) shows the density plot of the sensitivity index where the black and red regions represent highly sensitive regions that must be avoided.

7.1 Trade-Off Between Secondary Metrics. The contours of max. vertex distance and min. ground clearance are superimposed over the sensitivity index. The cognate members shown in Figs. 3(a) and 3(b) are marked in the Fig. 3(f). The members marked with triangles indicate points in the cognate space where at least one link length measures to zero. Given a candidate design of vertices A, B, C, D, F, G, H, P_0 , these four points correspond to the following stretch-rotation parameter values:

$$\begin{split} \sigma &= 0 \\ \sigma &= \frac{B - G}{B - D} \\ \sigma &= \frac{(D - F)(B - G)}{B(D - F) + D(F - G) + C(-D + G)} \\ \sigma &= \frac{B(G - H) + G(H - P_0) + D(-G + P_0)}{(B - D)(G - H)} \end{split}$$

Of these, the former two are degeneracies of the parametric family where one of the four-bar loops of the Watt mechanism collapses to a point. This explains why the neighborhood of these points are highly sensitive in Fig. 3(f). The latter two cases correspond to the lengths FC and HP_0 becoming zero, respectively. These points do not affect the sensitivity adversely. The last case is interesting for a different reason altogether. Because H and P_0 coincide in this design, the end effector point lies at the junction of two links as indicated in Fig. 4(a). Hence, the mechanism is simultaneously WI-C and WI-A. This opens up a new cognate Λ of WI-A shown in Fig. 4(b) which delivers the same timed motion. Note that while WI-A has four cognates in a generic group, two of them are always degenerate in this special construction and the only non-degenerate ones are shown in Fig. 4. Dijksman has noted the existence of this special relation between WI-A and WI-C in Ref. [2].

We present a second design family in Fig. 5 arrived through identical analysis. The path shown in Fig. 5(a) actually does not pass through P_2 and P_3 , which is imperceptible. The combined contour plot shows that this family offers a larger range of preferred designs compared to the earlier candidate. In particular, this family of designs provides for more compact mechanisms.

8 Summary

In this work, timed curve synthesis of Watt six-bar linkages is solved using a numerical continuation technique called random monodromy loops. The mathematical modeling is through the derivation of systems of polynomial equations. Four distinct cases of Watt mechanisms, WI-A, WI-B, WI-C, and WII are posed. The former two cases can satisfy up to eight precision points while the latter two can only satisfy seven. The maximum number of possible solutions, called the root count, is estimated for the system of equations using the continuation technique. Computational reductions are made possible by the existence of Watt cognates. To enable this, existing literature on geometric construction of Watt cognates is revisited, and simpler algebraic rules that mirror these constructions are presented. It is estimated that the root count is of the order of a million in WI-B and smaller in the other cases. These estimates are available in Table 1 for reference. Furthermore, a theory is offered in explanation of path failures for parameter

⁵The same grid is used for all subsequent analysis in this work.

homotopies that track from generic numerical space to systems with extra structure that represent physical dimensions.

For practical applications, WI-C (and WII to some extent) offers a natural advantage over WI-A, WI-B and even Stephenson linkages in terms of the availability of two free design choices. While this comes at the cost of a reduction in the number of precision points possible (seven as opposed to eight), it presents a readily available avenue for enforcing secondary design considerations. In this paper, secondary considerations are evaluated as a postanalysis step on a grid of the two free parameters of the WI-C. The trade-offs of three secondary performance metrics are illustrated, namely, max. vertex distance (to measure link compactness), min. ground clearance and sensitivity of the design output to errors in link dimensions.

Acknowledgment

The authors gratefully acknowledge the support of the National Science Foundation Award No. CMMI-2041789.

Conflict of Interest

There are no conflicts of interest.

Data Availability Statement

The authors attest that all data for this study are included in the paper.

References

- [1] Baskar, A., and Plecnik, M., 2021, "Synthesis of Six-Bar Timed Curve Generators of Stephenson-Type Using Random Monodromy Loops," ASME J. Mech. Rob., 13(1), p. 011005.
- [2] Dijksman, E., 1971, "Six-Bar Cognates of Watt's Form," J. Eng. Ind.: Trans. ASME, **93**(1), pp. 183–190.
- [3] Roberts, S., 1875, "On Three-Bar Motion in Plane Space," Proc. Lond. Math. oc., s1-7(1), pp. 14-23.
- [4] Wampler, C., Morgan, A., and Sommese, A., 1992, "Complete Solution of the Nine-Point Path Synthesis Problem for Four-Bar Linkages," ASME J. Mech. Des., **114**(1), pp. 153–159.
- , Sommese, A., and Wampler, C., 2011, "Regeneration Homotopies for Solving Systems of Polynomials," Math. Comput., 80(273), pp. 345-377.
- [6] Bates, D. J., Hauenstein, J. D., Sommese, A. J., and Wampler, C. W., 2013, Numerically Solving Polynomial Systems With Bertini, SIAM, Philadelphia.
- [7] Freudenstein, F., 1954, "An Analytical Approach to the Design of Four-Link Mechanisms," Trans. ASME, 76(3), pp. 483-492.
- [8] Erdman, A. G., and Sandor, G. N., 1971, "Kinematic Synthesis of a Geared Five-Bar Function Generator," ASME J. Eng. Ind., 93(1), pp. 11-16.

- [9] Krishnamurty, S., and Turcic, D. A., 1992, "Optimal Synthesis of Mechanisms Using Nonlinear Goal Programming Techniques," Mech. Mach. Theory, 27(5), pp. 599-612.
- [10] Cabrera, J., Simon, A., and Prado, M., 2002, "Optimal Synthesis of Mechanisms With Genetic Algorithms," Mech. Mach. Theory, 37(10), pp. 1165–1177.
 [11] Agarwal, S., and Bandyopadhyay, S., 2017, "Design of Six-Bar Function
- Generators Using Dual-order Structural Error and Analytical Mobility Criteria," Mech. Mach. Theory, 116, pp. 326-351.
- [12] Su, H.-J., and McCarthy, J. M., 2007, "Synthesis of Bistable Compliant Four-Bar Mechanisms Using Polynomial Homotopy," ASME J. Mech. Des., 129(10), pp. 1094-1098.
- [13] Plecnik, M. M., and Michael McCarthy, J., 2014, "Numerical Synthesis of Six-Bar Linkages for Mechanical Computation," ASME J. Mech. Rob., 6(3), p. 031012.
- [14] Plecnik, M. M., and McCarthy, J. M., 2016, "Computational Design of Stephenson II Six-Bar Function Generators for 11 Accuracy Points." ASME J. Mech. Rob., 8(1), p. 011017.
- [15] Jensen, P. W., 1992, "The Polode Synthesis Method," Forschung im Ingenieurwesen, 58(6), pp. 152-163.
- [16] Plecnik, M. M., and Fearing, R. S., 2020, "Designing Dynamic Machines With Large-Scale Root Finding," IEEE Trans. Rob., 36(4), pp. 1135-1152.
- [17] Lee, M.-Y., Erdman, A. G., and Faik, S., 1999, "A Generalized Performance Sensitivity Synthesis Methodology for Four-Bar Mechanisms," Mech. Mach. Theory, 34(7), pp. 1127–1139.
- [18] Hanzaki, A. R., Rao, P., and Saha, S., 2009, "Kinematic and Sensitivity Analysis and Optimization of Planar Rack-and-Pinion Steering Linkages," Mech. Mach. Theory, 44(1), pp. 42–56.
- [19] Wampler, C. W., 1996, "Isotropic Coordinates, Circularity, and Bézout Numbers: Planar Kinematics From a New Perspective," Proceedings of ASME Design Engineering Technical Conference and Computers in Engineering Conference, Irvine, CA, Aug. 18-22, pp. 139-155.
- [20] Plecnik, M. M., and McCarthy, J. M., 2016, "Kinematic Synthesis of Stephenson III Six-Bar Function Generators," Mech. Mach. Theory, 97, pp. 112-126.
- [21] Hauenstein, J. D., Oeding, L., Ottaviani, G., and Sommese, A. J., 2019, "Homotopy Techniques for Tensor Decomposition and Perfect Identifiability," J. für die reine und angewandte Mathematik (Crelles Journal), 2019(753), pp. 1-22.
- [22] Plecnik, M. M., and Fearing, R. S., 2017, "Finding Only Finite Roots to Large Kinematic Synthesis Systems," ASME J. Mech. Rob., 9(2), p. 021005.
- [23] Duff, T., Hill, C., Jensen, A., Lee, K., Leykin, A., and Sommars, J., 2018, 'Solving Polynomial Systems Via Homotopy Continuation and Monodromy," IMA J. Numer. Anal., 39(3), pp. 1421-1446.
- [24] Baskar, A., and Bandyopadhyay, S., 2019, "An Algorithm to Compute the Finite Roots of Large Systems of Polynomial Equations Arising in Kinematic Synthesis," Mech. Mach. Theory, 133, pp. 493-513.
- [25] Bates, D. J., Hauenstein, J. D., Sommese, A. J., and Wampler, C. W., Bertini:
- Software for Numerical Algebraic Geometry. [26] Hauenstein, J. D., and Sherman, S., 2020, "Using Monodromy to Statistically Estimate the Number of Solutions,". Springer Proceedings in Advanced Robotics, B. Siciliano, and O. Khatib, eds.
- Sherman, S. N., Hauenstein, J. D., and Wampler, C. W., 2020, "Curve Cognate Constructions Made Easy," Proceedings of the ASME 2020 International Design Engineering Technical Conferences and Computers and Information in Engineering Conference. Volume 10: 44th Mechanisms and Robotics Conference (MR), Virtual, Online, Aug. 17-19, American Society of Mechanical Engineers Digital Collection, p. V010T10A024.
- [28] Balli, S. S., and Chand, S., 2002, "Defects in Link Mechanisms and Solution Rectification," Mech. Mach. Theory, 37(9), pp. 851-876.
- McCarthy, J. M., and Soh, G. S., 2010, Geometric Design of Linkages, Vol. 11, Springer Science & Business Media, New York.
- [30] Beloiu, A. S., and Gupta, K. C., 1997, "A Unified Approach for the Investigation of Branch and Circuit Defects," Mech. Mach. Theory, 32(5),
- Wolfram Research, Inc., 2019, Mathematica, Version 12.1, Champaign, IL.